

Nonvolatile reconfigurable current divider based on spin extraction in lateral ferromagnet/nonmagnet transport structures

Yori Manzke,* Rouin Farshchi, Pawel Bruski, Jens Herfort, and Manfred Ramsteiner
Paul-Drude-Institut für Festkörperelektronik, Hausvogteiplatz 5-7, 10117 Berlin, Germany

(Received 13 November 2012; published 18 April 2013)

We demonstrate a device concept for a lateral spin-transport structure consisting of ferromagnetic (Co_2FeSi) stripes on a nonmagnetic (n -GaAs) transport channel. The basic building block of the device consists of a local spin valve which utilizes spin extraction instead of injection at the ferromagnetic contact stripes for its fundamental operation principle. An extended device comprises an array of such spin valves in which the spin polarization in the transport channel results from a cascade of spin extraction events. The achieved functionality can be described in terms of a nonvolatile reconfigurable current divider. We show that for m ferromagnetic contacts, 2^{m-1} electrical output levels can occur, where each output level corresponds to a particular magnetization configuration of the entire stripe array.

DOI: [10.1103/PhysRevB.87.134415](https://doi.org/10.1103/PhysRevB.87.134415)

PACS number(s): 85.75.-d, 72.25.Dc, 75.50.Bb, 75.76.+j

I. INTRODUCTION

The creation of a nonequilibrium spin polarization of conduction electrons in a semiconductor (SC) material is widely considered to be a prerequisite for semiconductor spintronic devices.¹ Various implementations^{2,3} take advantage of a shared interface of the SC with a ferromagnetic metal (FM). For example, a reverse-biased Schottky contact to a FM is frequently used to electrically inject spin-polarized electrons, which can be detected either optically^{4,5} or electrically, the latter in a nonlocal⁶ as well as in a local⁷⁻⁹ geometry. Spin reflection from the hybrid interface (also referred to as spin extraction) constitutes an additional means to generate a spin accumulation inside the SC,^{10,11} which can result from a photocurrent^{12,13} or an electrical forward bias.^{4,6,14,15} For the fundamental proof of spin extraction, optical techniques,^{4,12-14} and electrical schemes in the nonlocal geometry, in which spin diffusion is separated from the path of charge transport,^{6,15} have been applied. However, the majority of spintronic device concepts and related circuits require the use of spin-polarized charge currents rather than pure spin diffusion.¹⁶ For related applications—e.g., based on local spin valves—the utilization of spin extraction has so far been considered in theoretical device proposals only.^{10,17,18}

In this paper, we present a local magnetoresistance device based on spin extraction. In this spin extraction spin valve (SESV), a spin polarization is generated inside a nonmagnetic semiconductor by spin extraction at a forward-biased ferromagnetic contact. This spin polarization is detected locally using another forward-biased ferromagnetic contact. In addition, we show the extension of this concept to a functional spintronic circuit that comprises multiple extraction events. In such a multiple extraction spin valve (MESV) the electrical output is determined by a number of ferromagnetic input magnetizations.

II. EXPERIMENTAL

The samples under investigation are grown by molecular beam epitaxy on semi-insulating GaAs(001) substrates. A conductive channel is created by Si doping with a thickness of 1500 nm and a doping density of $n_{\text{channel}} = 2 \times 10^{16} \text{ cm}^{-3}$,

followed by a layer with a linearly increasing doping density of thickness 15 nm ranging from n_{channel} to $n_{\text{interface}} = 5 \times 10^{18} \text{ cm}^{-3}$ and a 15-nm-thick layer with $n_{\text{interface}}$. After transfer in ultrahigh vacuum into a growth chamber for metals, a 16-nm-thick layer of the ferromagnetic Heusler alloy Co_2FeSi is deposited epitaxially at a substrate temperature of 280 °C. The material system was previously found to yield efficient spin injection.^{21,22} Further details about the growth of Co_2FeSi on GaAs(001) can be found, e.g., in Refs. 23 and 24. A $50 \times 400 \mu\text{m}^2$ conductive mesa region with ferromagnetic stripe contacts, which we denote A, B, C, and D with widths 10, 8, 10, and 12 μm , respectively, is defined by optical lithography. The edge-to-edge spacing between B and C as well as between C and D is 14 μm (3 μm) for sample 1 (sample 2), while the spatial separation between A and B ($\sim 145 \mu\text{m}$) is much larger than the spin-relaxation length [cf. Fig. 1(a)]. The impact of drift on the spin-relaxation length has been revealed by spin-valve measurements with varying stripe distances (not shown here). The effective spin-relaxation length (in the following denoted as spin drift length) has been found to be increased in local spin valve experiments by almost a factor of 2 as compared to nonlocal measurements where drift does not play a role. Contact A serves as a source of unpolarized electrons, while contacts B, C, and D are used for extraction and/or detection of electron spins. The electrical measurements rely on a standard dc method, wherein currents are determined from nanovoltmeter readings of voltage drops across an ohmic resistor with a resistance of 82.4 Ω . All measurements are performed at 40 K in a He exchange gas cryostat.

III. RESULTS AND DISCUSSION

A. Spin extraction spin valve

Spin extraction is the essential physical process needed for the operation of our SESV devices. To demonstrate that spin extraction at a ferromagnetic contact leads to an exploitable polarization for spin valve operations, we utilize the configuration depicted schematically in Fig. 1(b). An unpolarized electron current is injected into an n -type GaAs channel at stripe A, whereas stripes B and C serve as a pump-and-probe arrangement, i.e., the degree of spin extraction at

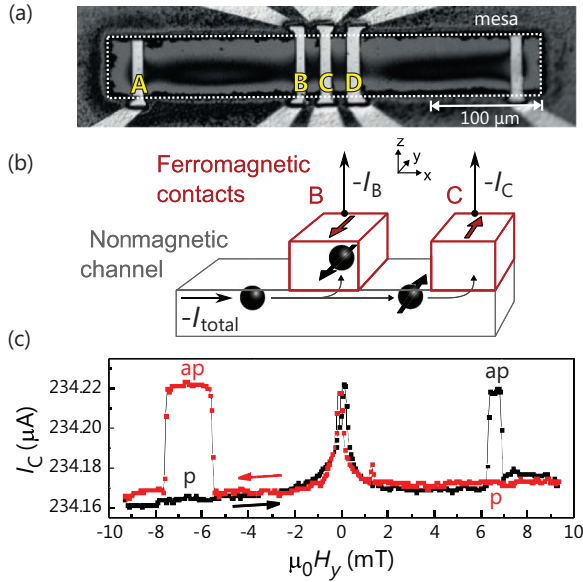


FIG. 1. (Color online) (a) Optical micrograph of sample 1. (b) Schematic representation of a spin extraction experiment, with ferromagnetic electrodes B and C. Black arrows indicate the direction of net electron flow. (c) Output current I_C as a function of the in-plane magnetic field (applied along the ferromagnetic easy axis) for $I_{total} = 500 \mu A$ at 40 K. Note that the switching field is of a stochastic nature, as seen from the different peak widths at positive and negative fields (Ref. 19). The feature at $H_y = 0$ is attributed to dynamic nuclear polarization (Ref. 20).

contact B is detected at stripe C via a spin-dependent contact resistance. In this current divider, a current source supplies a constant I_{total} , such that electrons flow into both B and C stripes in a parallel manner. Since the spatial separation between stripes A and B exceeds the spin drift length in GaAs, the electron current is unpolarized when reaching contact B.

The partial current I_C measured in sample 1 is shown in Fig. 1(c) as a function of the external magnetic field $\mu_0 H_y$ applied along the easy axis of magnetization of the ferromagnetic stripes. Due to the different coercivities of the FM electrodes the system undergoes a switching sequence from a parallel (p) to an antiparallel (ap) configuration and back to a parallel configuration upon sweeping the field. Accordingly, we observe the switching of I_C upon magnetization reversal of the FM stripes. This is an indication of magnetoresistance mediated by a spin polarization of the conduction electrons inside the semiconductor. The observed behavior is explained by a contact resistance of the probe stripe C which depends on the orientation of this spin polarization relative to the magnetization of stripe C. Obviously, the origin of the electron polarization is a spin-generation process at the pump stripe B. In contrast to the case of spin injection at contact B (see local spin-valve experiment described below), the resistance at stripe C decreases in the ap configuration, i.e., the spin polarization generated at the forward-biased FM/SC contact of stripe B is antiparallel to that generated by spin injection. This observation identifies spin extraction as the generation process at stripe B. Our measurements demonstrate that the electron polarization induced by spin extraction is sufficient to observe

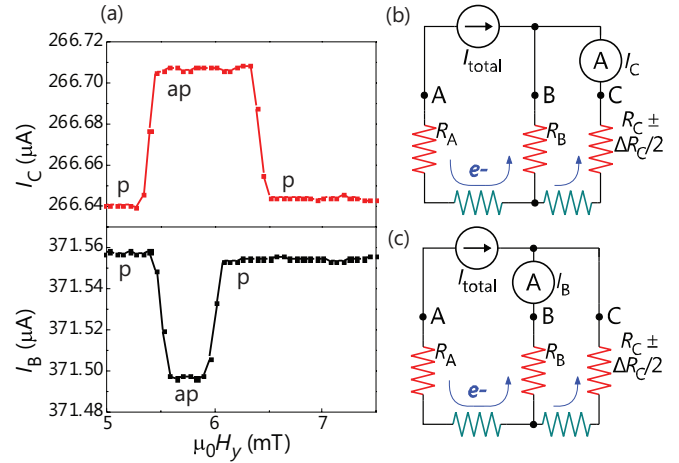


FIG. 2. (Color online) (a) Current versus applied field for output leads C (top) and B (bottom) with $I_{total} = 600 \mu A$ (sample 1) measured in separate runs. “p” and “ap” indicate the parallel and antiparallel magnetization configurations of B and C. (b) and (c) show simplified circuit diagrams for measurements of I_C and I_B , respectively. The contact resistances are represented by ohmic resistors (red), and the horizontal resistors (green) represent the resistance of the semiconductor channel. ΔR_C denotes the spin dependence of the contact resistance, and the blue arrows indicate the direction of net electron flow.

a clear local spin-valve effect between the ferromagnetic stripes B and C.

A comparison of the field dependence of the output currents through contacts B and C is shown in Fig. 2(a) for two separate measurements. While I_C switches to a higher current state for an antiparallel magnetization configuration, I_B is found to be reduced for this configuration. This observation can be explained by a magnetization-dependent change in contact resistance at C, as depicted in Figs. 2(b) and 2(c). The model circuits use an Ohmic approximation of all contact resistances. The current is unpolarized prior to the extraction event at contact B and thus experiences no magnetization-dependent resistance at that contact, whereas the polarized current into C leads to a spin-dependent resistance $R_C \pm \Delta R_C/2$. A higher (lower) contact resistance corresponds to the parallel (antiparallel) magnetization configuration of B and C.

The dependence of the spin extraction signal on the applied current is depicted in Fig. 3. The jumps in current

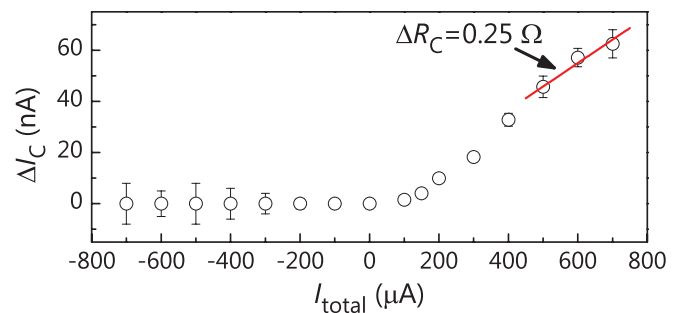


FIG. 3. (Color online) Output current changes ΔI_C with applied current I_{total} (sample 1). The red solid line is the calculated current change resulting from a contact resistance change of $\Delta R_C = 0.25 \Omega$.

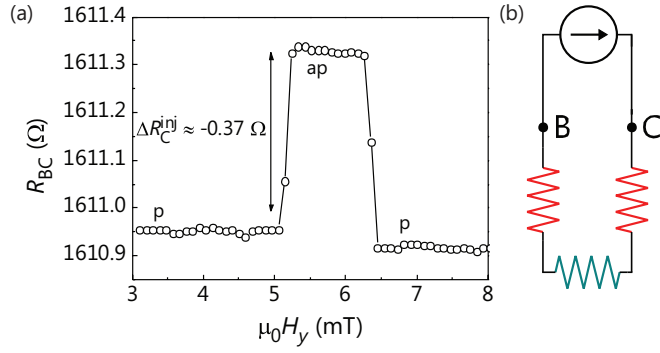


FIG. 4. (Color online) (a) Local spin-valve resistance R_{BC} vs $\mu_0 H_y$ for contacts B and C on sample 1. (b) shows the corresponding circuit diagram.

upon magnetization reversal, $\Delta I_C = I_{C,ap} - I_{C,p}$, are seen to increase monotonically with I_{total} . When the electron flow is reversed, i.e., for a net electron flow from B and C into the faraway contact A, we observe no spin-dependent signals, which indicates that spin injection at B is not appreciably affected by a spin imbalance in the semiconductor channel. We analyze Kirchhoff's rules for the simple parallel circuit depicted in Fig. 2(b) to extract the spin-dependent part of the contact resistances ΔR_C from the measured current changes. All resistances in the model circuit are approximated to be Ohmic²⁵ and are estimated from pairwise measurements of $I-V$ curves between all contacts. ΔR_C is found to be about 0.25Ω for $500 \mu A \leq I_{total} \leq 700 \mu A$.

To quantify the efficiency of spin generation by extraction, we compare the spin-dependent contact resistances (ΔR_C) for two cases: spin extraction (ΔR_C^{extr}) and spin injection (ΔR_C^{inj}) at contact B. For the injection we measure the local magnetoresistance between B and C with all other leads disconnected (Fig. 4). Such a local spin valve (LSV) experiences a voltage change for a constant applied current when the magnetization directions of the electrodes undergo a transition between the parallel and antiparallel configurations. This can be described by a change in contact resistance at contact C due to spin injection at contact B. The magnetoresistance $\Delta R = R_p - R_{ap}$ is then estimated as $\Delta R_C^{inj} = -0.37 \Omega$ for an applied current of $266 \mu A$. For both the LSV and the SESV, the spin-dependent resistances can be approximated by

$$\Delta R_C^{extr/inj} = S_C^{extr/inj} \delta = S_B^{extr/inj} e^{-d/\lambda_S} \delta,$$

where $S_B^{extr/inj}$ ($S_C^{extr/inj}$) denote the electron spin polarizations arriving at contact B (C) generated by extraction or injection, λ_S denotes the spin drift length in the SC, d denotes the separation between contacts B and C, and δ a quantity proportional to the detection efficiency. Since the detection mechanism is the same for the LSV and the SESV, we can compare the spin generation efficiencies $\eta^{extr/inj} \propto S_B^{extr/inj}$,

$$\eta^{extr}/\eta^{inj} = \Delta R_C^{extr}/\Delta R_C^{inj} \cong -0.7.$$

From this estimate, two important results can be deduced: First, the spin generation by extraction is of a comparable efficiency as the spin generation by spin injection. Second, the nonequilibrium spin polarization resulting from a forward bias

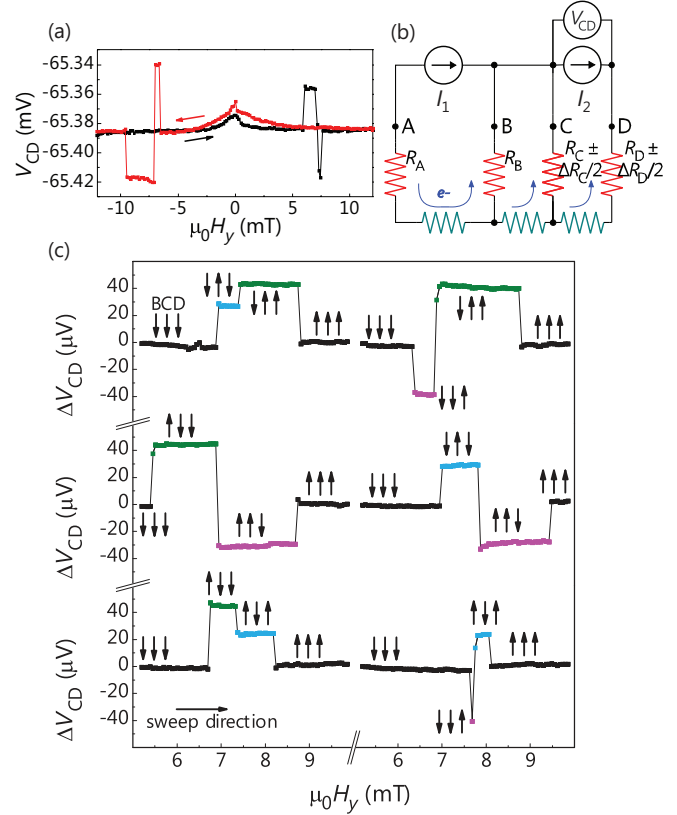


FIG. 5. (Color online) (a) shows the output voltage V_{CD} of a double extraction spin valve upon sweeping $\mu_0 H_y$ for sample 2 with $I_1 = 400 \mu A$ and $I_2 = 50 \mu A$. The circuit schematic is depicted in (b). (c) shows all six sequences of the output voltage changes ΔV_{CD} with sweeping $\mu_0 H_y$. The corresponding magnetization configurations are indicated by black arrows.

across the Schottky contact exhibits an opposite sign compared to a reverse bias, which confirms our expectation.

B. Multiple extraction spin valve

The spin extraction experiment depicted above can be regarded as a building block of an extended device with a more complex functionality, which we will refer to as a MESV. Data is shown in Fig. 5(a) for sample 2 in a geometry that comprises three ferromagnetic output electrodes, as depicted in Fig. 5(b). Here, the electrical current flows from the remote contact A into the contacts B, C, and D in a parallel manner. Again, the extracted spin information from contact B is sensed by contact C. An additional contact D then senses the extracted spins from both B and C. The measurement of V_{CD} across the additional current source I_2 has the advantage of a higher sensitivity to spin-dependent changes in resistance at contacts C and D and yields a lower noise level in our experiments. However, qualitatively equivalent data can be obtained for the output current I_D measured without the additional current source I_2 (not shown here). As seen from Fig. 5(a), we can access three output voltage levels by sweeping the field from negative to positive ferromagnetic saturation. Each voltage level corresponds to a particular magnetization configuration of contacts B, C, and D. The order of magnetization reversals again occurs in a stochastic manner. As a consequence, we

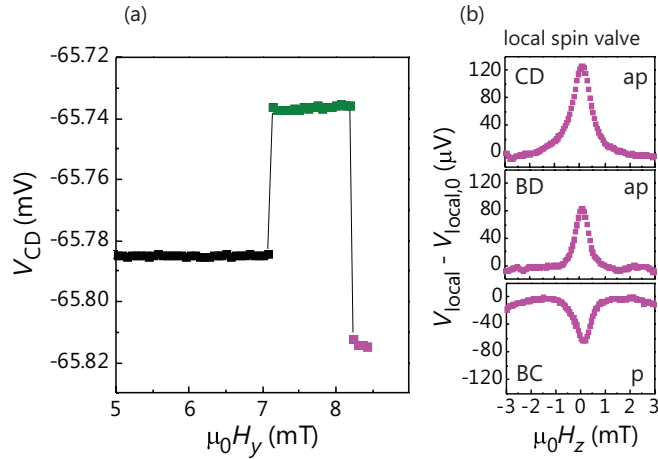


FIG. 6. (Color online) Hanle-effect measurements of the double extraction spin valve (sample 2). (a) shows an aborted measurement of V_{CD} upon sweeping $\mu_0 H_y$. (b) depicts Hanle voltages V_{local} as a function of the out-of-plane field $\mu_0 H_z$ in the local geometry for the denoted electrode pairs with a subtracted background voltage $V_{local,0}$.

can observe all six possible sequences of single switching events that lead to a complete reversal of the magnetization configuration from $\downarrow\downarrow\downarrow$ (BCD) to $\uparrow\uparrow\uparrow$, depicted in Fig. 5(c). Four output levels are observed, as indicated by colors.

To assign the corresponding magnetization configurations [denoted by the black arrows in Fig. 5(c)] to the different output levels, we investigate spin dephasing in the Hanle geometry with a magnetic field applied out of the sample plane, which corresponds to the magnetic hard axis of the FM contacts and thus the in-plane magnetization is maintained for the applied magnetic fields. An example of such Hanle measurements is shown in Fig. 6. First, the output level of interest is prepared by aborting a sweep of the in-plane magnetic field $\mu_0 H_y$ in the MESV configuration [cf. Fig. 6(a)]. Then, Fig. 6(b) depicts the local voltages for a constant applied current of $400 \mu\text{A}$ in an LSV arrangement as a function of $\mu_0 H_z$ for the denoted electrode pairs. The observed Hanle curve shapes allow for a mutual determination of the relative magnetizations of B, C, and D. More specifically, spin dephasing with increasing field leads to a peak (dip) at $H_z = 0$ for an antiparallel (parallel) magnetization orientation of the two contacts. Consequently, the magnetization configuration $\uparrow\uparrow\downarrow$ (BCD) is deduced for the aborted output level. All other magnetization configurations can be assigned to their corresponding voltage levels in the same way.

The output levels ΔV_{CD} in Fig. 5(c) can be explained quantitatively by regarding a simple model circuit shown in Fig. 5(b). Table I shows the measured output voltages and the corresponding calculated spin-induced contact resistance changes for all configurations using a realistic set of parameters.²⁶ The circuit model is consistent with the experimental data within the sensible restrictions that (a) the contact resistance of C is dependent on the relative orientation of the magnetizations of B and C (high for parallel, low for antiparallel), and (b) the spin dependence of the contact resistance of D is dominated by the relative magnetization orientation of C and D.

Furthermore, using a simple model for spin transport (see the Appendix), which involves the spin extraction efficiency (η^{extr}) and the spin drift length (λ_S) as the only adjustable parameters, we can connect the contact resistances ΔR_C and ΔR_D to the incoming spin polarizations S_C and S_D to confirm our model of multiple spin extraction. Based on nonlocal spin-valve measurements in similar device structures, we have chosen $\eta^{\text{extr}} = 16\%$ and $\lambda_S = 11 \mu\text{m}$ as realistic parameters. These values yield spin polarizations that are proportional to the corresponding absolute values of ΔR_C and ΔR_D within the experimental error, where the sign of ΔR_C and ΔR_D is determined by the relative orientation of the spin polarization and the contact magnetization (see Table I). Note that the observation $\Delta R_D > \Delta R_C$ for the magnetizations B and C being parallel indicates an increased spin polarization induced by the cascade of two extraction events. The same relative change of the spin polarizations ($S_D > S_C$) is obtained by our simple transport model. For an increased amount of ferromagnetic stripes comprising parallel magnetization orientations, the same model predicts that a highly spin-polarized drift current should be achievable by multiple spin extraction.²⁷ Note that the predicted substantial enhancement of spin polarization requires a device size which does not exceed a few spin drift lengths. However, further experiments on MESVs containing a larger number of stripes are needed to verify this prospect.

Generally, in a MESV nonvolatile input magnetization states are used to control an output voltage or current, which can be measured in each of the output leads. Consequently, the concept of multiple spin extraction and detection opens up the possibility for multilevel logic functionality. In a scaled-up device with m ferromagnetic electrodes as binary inputs one obtains 2^{m-1} output states due to the fact that all FM electrodes but the first act in a dual role as spin detectors and generators. For such kind of MESV devices one has to consider that an increased number of output electrodes results in a reduced spin signal in one particular contact, which potentially imposes challenges on the sensitivity of the detection. Note that the symmetrically equivalent magnetization configurations (such as $\downarrow\uparrow\downarrow$ and $\uparrow\downarrow\uparrow$ in Table I) share a common output level. Therefore, unique assignment of an electrical output level to its corresponding magnetization configuration requires the knowledge of one input magnetization.

One potential application of the MESV is the readout of magnetic data. The magnetization directions of the ferromagnetic electrodes can be regarded as an array of stored

TABLE I. Experimental double extraction spin-valve output levels ΔV_{CD} [see Fig. 5(c)], spin-dependent contact resistances, and spin-polarization values deduced from modeling. The upper (lower) sign of S_C and S_D corresponds to the magnetization state \uparrow (\downarrow) of contact B.

Conf. (BCD)	$\uparrow\uparrow\uparrow, \downarrow\downarrow\downarrow$	$\uparrow\uparrow\downarrow, \downarrow\downarrow\uparrow$	$\uparrow\downarrow\uparrow, \downarrow\uparrow\downarrow$	$\uparrow\downarrow\downarrow, \downarrow\uparrow\uparrow$
ΔV_{CD} (Expt.)	0 by def.	$(-34 \pm 4) \mu\text{V}$	$(27 \pm 3) \mu\text{V}$	$(43 \pm 2) \mu\text{V}$
ΔR_C	0.62Ω	0.62Ω	-0.62Ω	-0.62Ω
ΔR_D	0.68Ω	-0.68Ω	-0.32Ω	0.32Ω
S_C	± 0.054	± 0.054	± 0.054	± 0.054
S_D	± 0.059	± 0.059	∓ 0.030	∓ 0.030

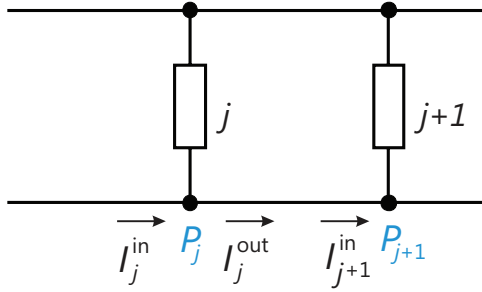


FIG. 7. (Color online) Current divider schematic for spin-transport model. See text for an explanation of the labels.

information. Since the electrical output state of a MESV reflects the magnetization configuration of the entire system, an array of magnetic bits can be read by performing only one measurement. This concept might allow for a comparably simple cell architecture and circuit design compared to conventional magnetoresistive random access memory.

IV. CONCLUSION

In conclusion, the local electrical detection of electron spins generated at a forward-biased SC/FM Schottky contact by spin extraction is demonstrated. This concept constitutes a magnetoresistance device, which we refer to as a spin extraction spin valve. Also, we demonstrate an extended spin-valve device based on multiple extraction, which appears to be promising for potential spintronic applications.

ACKNOWLEDGMENTS

We thank Paulo Santos for a careful reading of the manuscript as well as Angela Riedel, Walid Anders, and Gerd Paris for technical assistance. Financial support from the DFG via SPP 1538 is gratefully acknowledged.

APPENDIX

To describe spin transport in our MESV devices, we consider two subsequent ferromagnetic stripes j and $j+1$ in a multistripe structure, as shown in Fig. 7. The incoming electron current I_j^{in} at node P_j is characterized by the partial

currents $\uparrow I_j^{\text{in}}$ and $\downarrow I_j^{\text{in}}$ of opposite spin polarization and the corresponding polarization S_j^{in} ,

$$I_j^{\text{in}} = \uparrow I_j^{\text{in}} + \downarrow I_j^{\text{in}}, \quad (\text{A1})$$

$$S_j^{\text{in}} = \frac{\uparrow I_j^{\text{in}} - \downarrow I_j^{\text{in}}}{\uparrow I_j^{\text{in}} + \downarrow I_j^{\text{in}}}. \quad (\text{A2})$$

The outgoing electron current I_j^{out} at P_j is assumed to be generated by a spin-dependent reflection at the ferromagnetic stripe j . The resulting spin extraction is given by the reflection coefficient η ,

$$\uparrow I_j^{\text{out}} = a(1 \pm \eta)\uparrow I_j^{\text{in}}, \quad (\text{A3})$$

$$\downarrow I_j^{\text{out}} = a(1 \mp \eta)\downarrow I_j^{\text{in}}, \quad (\text{A4})$$

with the sign on the right side of the expression given by the relative orientation of the electron polarization and the magnetization orientation of stripe j . The factor a accounts for a change in absolute current. The electron polarization S_j^{out} of the outgoing current at P_j ,

$$S_j^{\text{out}} = \frac{\uparrow I_j^{\text{out}} - \downarrow I_j^{\text{out}}}{\uparrow I_j^{\text{out}} + \downarrow I_j^{\text{out}}}, \quad (\text{A5})$$

is subject to spin relaxation which leads to a reduced polarization of the incoming electron current at P_{j+1} ,

$$S_{j+1}^{\text{in}} = S_j^{\text{out}} e^{-d_j/\lambda_S}, \quad (\text{A6})$$

where d_j is the distance between stripes j and $j+1$ and λ_S is the spin drift length. Normalizing the incoming electron current at P_{j+1} , the resulting partial currents are given by

$$\uparrow I_{j+1}^{\text{in}} = \frac{1}{2}(S_{j+1}^{\text{in}} + 1), \quad (\text{A7})$$

$$\downarrow I_{j+1}^{\text{in}} = 1 - \uparrow I_{j+1}^{\text{in}}. \quad (\text{A8})$$

Note that we regard dimensionless currents since we are eventually interested in the spin polarizations only. Finally, we expect the resistance change at stripe $j+1$ to be proportional to the polarization of the incoming electron current:

$$\Delta R_{j+1} = c S_{j+1}^{\text{in}}. \quad (\text{A9})$$

Using a proportionality constant of $c = 11 \Omega$ together with $\eta = 16\%$ and $\lambda_S = 11 \mu\text{m}$, we achieve very good agreement with the experimental data given in Table I.

*manzke@pdi-berlin.de

¹*Handbook of Spin Transport and Magnetism*, edited by E. Y. Tsymlal and I. Žutić (Chapman and Hall/CRC, London, 2011).

²K. Ando, S. Takahashi, J. Ieda, H. Kurebayashi, T. Trypiniotis, C. H. W. Barnes, S. Maekawa, and E. Saitoh, *Nature Mater.* **10**, 655 (2011).

³J.-C. Le Breton, S. Sharma, H. Saito, S. Yuasa, and R. Jansen, *Nature (London)* **475**, 82 (2011).

⁴S. A. Crooker, M. Furis, X. Lou, C. Adelman, D. L. Smith, C. J. Palmström, and P. A. Crowell, *Science* **309**, 2191 (2005).

⁵H. J. Zhu, M. Ramsteiner, H. Kostial, M. Wassermeier, H.-P. Schönherr, and K. H. Ploog, *Phys. Rev. Lett.* **87**, 016601 (2001).

⁶X. Lou, C. Adelman, S. A. Crooker, E. S. Garlid, J. Zhang, K. S. M. Reddy, S. D. Flexner, C. J. Palmström, and P. A. Crowell, *Nat. Phys.* **3**, 197 (2007).

⁷M. Ciorga, C. Wolf, A. Einwanger, M. Utz, D. Schuh, and D. Weiss, *AIP Advances* **1**, 022113 (2011).

⁸P. Chen, J. Moser, P. Kotissek, J. Sadowski, M. Zenger, D. Weiss, and W. Wegscheider, *Phys. Rev. B* **74**, 241302 (2006).

⁹K. Kasahara, Y. Baba, K. Yamane, Y. Ando, S. Yamada, Y. Hoshi, K. Sawano, M. Miyao, and K. Hamaya, *J. Appl. Phys.* **111**, 07C503 (2012).

- ¹⁰C. Ciuti, J. P. McGuire, and L. J. Sham, *Phys. Rev. Lett.* **89**, 156601 (2002).
- ¹¹V. V. Osipov and A. M. Bratkovsky, *Phys. Rev. B* **72**, 115322 (2005).
- ¹²R. K. Kawakami, Y. Kato, M. Hanson, I. Malajovich, J. M. Stephens, E. Johnston-Halperin, G. Salis, A. C. Gossard, and D. D. Awschalom, *Science* **294**, 131 (2001).
- ¹³R. J. Epstein, I. Malajovich, R. K. Kawakami, Y. Chye, M. Hanson, P. M. Petroff, A. C. Gossard, and D. D. Awschalom, *Phys. Rev. B* **65**, 121202 (2002).
- ¹⁴J. Stephens, J. Berezovsky, J. P. McGuire, L. J. Sham, A. C. Gossard, and D. D. Awschalom, *Phys. Rev. Lett.* **93**, 097602 (2004).
- ¹⁵X. Lou, C. Adelman, M. Furis, S. A. Crooker, C. J. Palmström, and P. A. Crowell, *Phys. Rev. Lett.* **96**, 176603 (2006).
- ¹⁶I. Žutić, J. Fabian, and S. Das Sarma, *Rev. Mod. Phys.* **76**, 323 (2004).
- ¹⁷R. K. Kawakami, K. McCreary, and Y. Li, in *Nanoelectronics and Photonics: From Atoms to Materials, Devices, and Architectures*, edited by A. Korkin and F. Rosei (Springer, New York, 2008), Chap. 5, pp. 59–114.
- ¹⁸H. Dery and L. J. Sham, *Phys. Rev. Lett.* **98**, 046602 (2007).
- ¹⁹G. Salis, A. Fuhrer, R. R. Schlittler, L. Gross, and S. F. Alvarado, *Phys. Rev. B* **81**, 205323 (2010).
- ²⁰G. Salis, A. Fuhrer, and S. F. Alvarado, *Phys. Rev. B* **80**, 115332 (2009).
- ²¹M. Ramsteiner, O. Brandt, T. Flissikowski, H. T. Grahn, M. Hashimoto, J. Herfort, and H. Kostial, *Phys. Rev. B* **78**, 121303 (2008).
- ²²P. Bruski, S. C. Erwin, M. Ramsteiner, O. Brandt, K.-J. Friedland, R. Farshchi, J. Herfort, and H. Riechert, *Phys. Rev. B* **83**, 140409 (2011).
- ²³M. Hashimoto, J. Herfort, H.-P. Schönherr, and K. H. Ploog, *Appl. Phys. Lett.* **87**, 102506 (2005).
- ²⁴M. Hashimoto, J. Herfort, H.-P. Schönherr, and K. H. Ploog, *J. Appl. Phys.* **98**, 104902 (2005).
- ²⁵ $R_B = R_C = 513 \Omega$, GaAs channel resistance between contacts B and C: $R_{Ch} = 75 \Omega$.
- ²⁶ $V_{CD} = \frac{(R_C + \Delta R_C/2)(I_2 - I_1)R_B + I_2 R_{Ch1}}{R_B + R_C + \Delta R_C/2 + R_{Ch1}} + I_2(R_D + \frac{\Delta R_D}{2} + R_{Ch2})$, $R_B = R_C = R_D = 825 \Omega$, channel resistances between B and C as well as between C and D: $R_{Ch1} = R_{Ch2} = 175 \Omega$.
- ²⁷Y. Manzke, R. Farshchi, P. Bruski, J. Herfort, and M. Ramsteiner, *IEEE Trans. Magn.* **49**(7) (2013), doi: 10.1109/TMAG.2013.2243712.